Derfi *et al. Cancer Cell International* (2024) 24:412
https://doi.org/10.1186/s12935-024-03609-6

Cancer Cell International

RESEARCH Open Access

Mithramycin targets head and neck cancer stem cells by inhibiting Sp1 and UFMylation

Kristina Vukovic Derfi[1], Tea Vasiljevic[1], Tea Dragicevic[1] and Tanja Matijevic Glavan[1*]

Abstract

Background The development of resistance to therapy is characteristic of head and neck squamous cell carcinoma (HNSCC), the 6th most common cancer, and is often attributed to cancer stem cells (CSCs). By proteomic approach, we determined that UFMylation plays an important role in HNSCC CSCs. Because of the necessity for innovative therapeutic strategies, we explore here the therapy targeting CSCs based on mithramycin and its inhibitory effect on Sp1 transcription factor, UFMylation, and CSCs survival and stemness.

Methods HNSCC-derived cancer cell lines Detroit 562, FaDu, and Cal27, and tumor spheres are used as a model for CSCs. Proteomic analysis identified the importance of the UFMylation pathway in CSCs which we further studied by bioinformatics, western blot, immunocytochemistry, and cytotoxicity assay.

Results Proteomic analysis and subsequent confirmation revealed UFSP2 and DDRGK1 were strongly expressed in tumor spheres. Bioinformatic analysis indicated high expression of UFM1 is linked with worse overall and disease-free survival, and it correlated with main EMT proteins (Zeb, Twist, and Fn) in HNSCC. UFM1 was also strongly expressed in tumor spheres compared to the adherent cells. Silencing of UFM1 reduced sphere number, size, and stemness. As Sp1 is the main transcription factor for the genes of the UFMylation system, we explored its inhibitor mithramycin, as a potential drug for CSCs inhibition. We proved mithramycin inhibits CSCs survival, induces apoptosis, and reduces UFMylation and stemness.

Conclusion UFMylation is an important process in CSCs, and mithramycin, or its lesser toxic analogs, should be further explored as CSCs targeted therapy in HNSCC.

Keywords Cancer stem cells, Head and neck cancer, Proteomics, UFMylation, Mithramycin

Introduction

Cancer stem cells (CSCs) are a subpopulation of cells in tumors that are able to self-renew, differentiate, initiate tumor, and aid the tumor`s resistance to chemotherapy or radiotherapy. CSCs may derive from adult tissue-specific stem cells or progenitor cells; however, they can also arise from differentiated cells due to genomic instability or hypoxia resulting in their dedifferentiation. At first, there were two main models of tumorigenesis, one named stochastic or clonal evolution, which presumed that a tumor consists of a heterogenous population of cells, in which each of them possesses the equal probability to initiate and promote tumor growth, and the hierarchy or CSC model, which assumed only a small population of cells within a tumor can drive tumor growth. Nonetheless, it has become evident that CSCs manifest a significant level of plasticity within a tumor microenvironment, recently described in an alternative model of cellular plasticity.

*Correspondence:
Tanja Matijevic Glavan
tmatijev@irb.hr
[1]Laboratory for Personalized Medicine, Division of Molecular Medicine, Rudjer Boskovic Institute, Bijenicka 54, Zagreb 10000, Croatia

This model unifies the stochastic and hierarchical models and presumes that there is a bidirectional interconversion between stem cells and non-stem-like states which contributes to tumor progression and therapeutic resistance.

This CSC plasticity is driven by the tumor microenvironment and/or genetic alterations. Specific markers that distinguish CSCs from cancer cells, or enrich their population are: CD44, CD133, CD24, CD90, and aldehyde dehydrogenase1 (ALDH1). Cancer cells gain stem-like characteristics through epithelial-mesenchymal transition (EMT), which is driven by different transcription factors, including Twist1/2, ZEB1/2, and Snai1/2. Head and neck cancer is the sixth most prevalent cancer globally and is characterized by its frequent post-treatment recurrence. Tobacco use, alcohol consumption, and human papillomavirus (HPV) infection are the primary etiological factors. A significant number of individuals exhibit suboptimal responses to therapeutic interventions, resulting in recurrent disease, which is often attributed to CSCs. The specific markers and properties of head and neck squamous cell carcinoma (HNSCC) CSCs have recently been discussed in a review [1].

Toll-like receptors (TLRs) are evolutionarily conserved receptors belonging to the family of pattern recognition receptors (PRRs) which play an important role in immune system. They recognize molecular patterns deriving from different pathogens and initiate immune responses. TLR3 binds dsRNA and is involved in viral RNA recognition and defense. However, recent research demonstrated that no external stimuli such as viral infection are necessary for TLR3 stimulation, but that necrotic cells within tumor tissue, dying of hypoxia or chemo-/radiotherapy can also induce TLR3 [2, 3]. Additionally, the role of TLR3 in cancer is still not clear: some studies suggest it should be exploited in cancer therapy as its activation leads to apoptosis [4], but other studies reveal its detrimental role in increasing tumor progression by either metabolic reprogramming [5, 6], or increased angiogenesis [7] and migration [8]. Additionally, one study so far has linked TLR3 activation with stem cell-like phenotypes in breast cancer cells [9].

The UFMylation pathway consists of recently discovered protein modifiers, similar to ubiquitination, that regulate a variety of biological processes by post-translationally attaching to proteins. Ubiquitin Fold Modifier-1 (UFM1) is a ubiquitin-like modifier (UBL) that is post-translationally attached to lysine residues on substrates through a system of enzymes conserved in most eukaryotes: Ubiquitin Like Modifier Activating Enzyme 5 (UBA5), Ubiquitin-Fold Modifier Conjugating Enzyme 1 (UFC1), and UFM1 Specific Ligase 1 (UFL1) identified as the E1, E2, and E3 enzymes respectively, while UFM1 Specific Peptidase 1 (UFSP1) and UFM1 Specific Peptidase 2 (UFSP2) are the UFM1-specific proteases [10]. It is also important to emphasize that the UFMylation process is reversible, so UFSPs can also cleave UFM1 from the substrate protein, thereby enabling the recycling of both UFM1 and its substrate. Even though the mutations in the genes coding for proteins of the UFM1 pathway are associated with several diseases, the functional importance of UFMylation remains elusive. It is known that UFMylation is linked to ER homeostasis, DNA damage response, p53 stabilization, protein biogenesis and regulation, and others [11–14]. The role of UFMylation in cancer is still unknown and contradictory results were obtained, depending on the cancer type. It is important to note that a large number of amplifications and deletions of genes encoding proteins involved in this process have been observed in tumors [15]. In certain tumors, the implicated proteins are considered oncogenes, while in others they play the role of tumor suppressors. In breast cancer estrogen receptor α is a target of UFMylation which stabilizes it by inhibiting its ubiquitination. This results in increased proliferation of tumor cells [16]. UFMylation has a similar effect in pancreatic adenocarcinoma. Wang et al. recently showed that the level of UFMylation is 2–3 times higher in the tumor than in the surrounding tissue [17]. In breast cancer, metformin downregulated SLC7A11 expression by inhibiting UFMylation of SLC7A11 resulting in ferroptosis [18]. In gastric cancer, UFBP1 increases the sensitivity of cancer cells to cisplatin by promoting proteasomal degradation of oxidative stress-response transcription factor Nrf2 [19]. Although more and more research has been done in recent years, little is still known about the role of UFMylation in cancer.

The development of resistance to therapy, the presence of distant metastases at diagnosis, and the significant morbidity are characteristic of HNSCC and emphasize the necessity for innovative therapeutic strategies. The treatment targeted towards CSCs is of great importance because classical chemo- or radiotherapy only reduces tumor bulk, while CSCs may enter quiescence and avoid therapy. Therefore, in this study, we have tried to determine the role of UFMylation in HNSCC CSCs and explore the potential of mithramycin as a CSC-targeted therapy, but also uncover its effect on UFMylation.

Materials and methods

Cells and reagents

The human HNSCC-derived cell lines FaDu, Detroit 562, and Cal27 were maintained in Dulbecco's modified Eagle medium (DMEM, Life technologies, Gaithersburg, USA) supplemented with 2mM L-glutamine and 10% fetal bovine serum (FBS) in a humidified chamber at 37 °C in 5% CO_2. Detroit 562 (batch No. 70004014) and FaDu (batch No. 63372030) cell lines were obtained from ATCC (LGC Standards) in 2018 (part of Head and Neck

Cancer Panel, TCP-1012). Polyinosinic-polycytidylic acid (poly(I: C)) and polyadenylic-polyuridylic acid (poly(A: U)) were obtained from InvivoGen (San Diego, USA). Doxycycline was purchased from Sigma Aldrich. Subclones of the FaDu cell lines were established by transfection with a plasmid carrying a shRNA directed against TLR3 and a doxycycline inducible promoter (TET-on system), thus allowing conditional knock-down of TLR3 as described previously and were a gift from Dr. Benjamin Verrilaud and prof. Pierre Busson [6]. Medium for tumor spheres was MEBM™ Mammary Epithelial Cell Growth Basal Medium (Lonza), supplemented with B-27™ Supplement (ThermoFisher Scientific), 20 ng/mL of Epidermal growth factor (EGF), and 10 ng/mL of Fibroblast growth factor (FGF) (Peprotech, UK). Tumor spheres were growing in low adhesion dishes.

For proteomic experiments, Detroit 562 cells were grown in low adhesion dishes to form tumor spheres for 3 days, then were treated for 24 h with pIC/pAU, followed by washing the cells with PBS for 3 times before the freezing of the pellets. Adherent cells were only seeded the day before.

Protein extraction and trypsin digestion

25 µL of SDS was added to 250 µL of the sample. The samples were then sonicated with ultrasound (5 min, cycles of 10 s of ultrasound, then 20 s of cooling). The sample was centrifuged for 10 min at 16,000 x g and 4 °C. The supernatant was separated and the precipitate was discarded. Protein concentration was determined by quantitative amino acid analysis using the Waters AccQ•Tag method according to the manufacturer's instructions (Waters). The method includes hydrolysis, derivatization of amino acids with AccQ•Fluor derivatization reagent and HPLC quantitative analysis. Hydrolysis was carried out for 24 h under vacuum at 114 °C. The resulting hydrolyzate was evaporated to dryness in a vacuum concentrator at 60 °C. After drying, the sample was dissolved in 20 µL of 20 mM HCl. Derivatization was carried out using AccQ-Fluor Reagent according to the manufacturer's instructions (Waters AccQTag Chemistry Package Instruction Manual). After derivatization, the samples were filtered through a 0.2 µm pore size filter. Separation and analysis of derivatized amino acids was performed according to the method described in the AccQ·Tag Chemistry Package Instruction Manual (Waters). The protein concentration in all samples was then adjusted to 1 mg/mL as follows: a sample volume containing 100 µg of protein was diluted with 35 mM TEAB buffer to a volume of 100 µL. 5 µL of 200 mM TCEP in 35 mM TEAB was added to the samples. The samples were incubated for 1 h at 55 °C. Then 5 µL of 375 mM IAA was added and the samples were incubated at room temperature for 30 min in a dark place. After the alkylation was finished, 6 volumes of ice-cold acetone were added to the samples. The samples were deposited overnight at -20 °C and then centrifuged for 10 min at 16,000 g and 4 °C. The acetone was discarded and the pellet resuspended in 100 µL digestion buffer (25 mM ammonium bicarbonate pH=7.8). Digestion in solution was performed with trypsin. 2 µL of trypsin (1 mg/mL concentration) was added to 100 µL of protein sample. Digestion was carried out by incubation in a thermomixer for 16 h at 37 °C and 700 rpm.

Tandem mass tag™ (TMT) labeling and high-performance liquid chromatography (HPLC) fractionation

Peptides obtained by digestion were labeled with isobaric labels (TMT simplex Isobaric Label reagent set) according to the manufacturer's instructions, and the labels of adherent control cells, control spheres and spheres treated with pAU and pIC were 126, 127, 128, and 129. This project had 4 groups, each group contained 3 biological replicate samples, a total of 12 samples. TMT labeling was performed according to the instructions of TMT Mass Tagging Kits and Reagents, Pub. No. MAN0011639.

Liquid chromatography-tandem mass spectrometry (LC–MS/MS) analysis

Peptide separation and mass spectrometry were performed using the SCIEX TripleTOF 6600+system equipped with Optiflow 1–50 µL Micro ion source (Sciex). Chromatographic separation was performed at 27 °C on a Phenomenex Luna Omega Polar Capillary, C18 column (3 µm, 150×0.3 mm) and using a Phenomenex Micro Trap C18 column (10×0.3 mm). The flow rate was set to 7 µL/min, and mobile phases A and B were 0.1% formic acid in water and 0.1% formic acid in acetonitrile, respectively.

The LC program was set as follows: 5–30% of B (0–68 min), 30–40% of B (68–73 min), 80% of B (73–78 min), 80−3% of B (78–79 min), and 3% of B (79–87 min). The ionization source operated in positive mode with following parameters: an ion spray voltage 4500 V, nebulizer gas 1 30 psi, nebulizer gas 2 35 psi and curtain gas 30 psi. The mass spectrometer scanned full spectra (*m/z* 400–1500) for 250 ms, followed by up to 50 MS/MS scans (*m/z* 100–2000). Candidate ions were isolated for fragmentation with a charge state between +2 and +5 and counts above a minimum threshold (100 counts per second). The rolling collision was employed with a collision energy spread of 5.

Bioinformatic analysis

After recording MS and MS/MS spectra, the obtained data were used for a database search using ProteinPilot Software 5.0.2 (AB Sciex). *Homo sapiens* proteome data were obtained from the UniProt database (entry number 26610; revised SwissProt sequences; accessed on August

1, 2022). Search parameters included one missed trypsin cleavage, carbamidomethylation and TMT6plex as a fixed modifications, with a precursor ion mass tolerance of 0.05 Da and fragment ion mass tolerance of 0.10 Da. The results were refined to include only proteins meeting the criteria of having a minimum of two identified peptide sequences and a false discovery rate (FDR) of less than 1%. The data obtained from the database search were then used for quantitative analysis. Median normalization and non-parametric statistical tests were applied for quantification, employing the Kruskal-Wallis test with Benjamini-Hochberg correction ($p<0.05$). Quantification was based on the reporter ion signal, and the analysis was performed by the Scaffold Q+S program 5.3.0. (Proteome Software). The complete table of altered proteins can be found in Supplementary data (Table 1).

The protein-protein interaction network was analyzed using STRING (http://www.strindb.org/). Parameters for String analysis included: Network type (full STRING network), required score (medium confidence (0.400)), and FDR stringency (medium (5%)). Panther knowledgebase was used to analyze datasets after proteomic analysis to find biological processes and protein classes. Transcription factors involved in the observed changes were determined by Funrich. We have also used GEPIA, a web server which extracts data from the Cancer Genome Atlas (TCGA) data portal and the GTEx database of normal tissues. http://gepia.cancer-pku.cn). We have used standard parameters. The "Harmonizome 3.0" web server was used to extract target genes of the SP1 transcription factor in ChIP-seq datasets from the ENCODE Transcription Factor Targets dataset.

Western blot

Cells were grown for 3 days in low adherence conditions with CSC medium to support tumor sphere formation and CSCs enrichment. Then they were treated with 10 µg/mL of pIC or pAU for 24 h after which the protein isolation followed.

Proteins were isolated and transferred onto 0.2 µm nitrocellulose membrane as described previously. The membranes were blocked with 5% BSA or 5% non-fat milk and were stained with primary antibodies: UFSP2 (1:1000, sc-376084, Santa Cruz Biotechnology, Inc.), GAPDH (1:1000, #5174, Cell Signaling Technology), PARP (1:1000, #9532, Cell Signaling Technology), DDRGK1 (1:3000, 21445-1-AP, Proteintech), UFL1 (1:1000, GTX120661, GeneTex) SP1 (1:300, sc-17824, Santa Cruz Biotechnology, Inc.).

Afterwards, the membranes were stained with an appropriate peroxidase conjugated secondary antibody, anti-rabbit IgG (1:5000, #7074, Cell Signaling Technology) and anti-mouse IgG (1:3000, NA931V, Amersham). The membranes were visualized with the chemiluminescent system (Perkin Elmer) and the Alliance Q9 Mini Chemiluminescence Imaging system (Uvitec Cambridge).

Transient transfection and RNA inhibition

Double-stranded small interfering RNA (siRNA) for knocking down the endogenous TLR3 (sc-36685), and UFM1 (sc-76804) including scrambled-sequence (control) siRNA (control siRNA-A, sc-37007), were obtained from Santa Cruz Biotechnology. For siRNA experiments, 70–80% confluent cells in 6 well dishes were transfected with TLR3 siRNA, UFM1 siRNA, or control siRNA (80 nM) using Transfectin reagent (Bio-Rad) according to the manufacturer's instructions. After 24 h, cells were seeded in low adhesion dishes in CSC medium and treated the next day with pIC/pAU for 24 h.

Immunocytochemistry

Detroit 562 cells were seeded in an 8-well chamber (Nunc® Lab-Tek® Chamber Slide™ system) at a density of 5×10^4 and grown overnight at 37 °C under 5% CO_2. 24 h after the treatment with 10 µg/mL poly(I: C) or poly(A: U), cells were washed with PBS followed by fixation with 4% fresh formaldehyde for 20 min, permeabilization with 0.3% Triton X-100 for 10 min, and blocking with 5% BSA for 45 min at room temperature. Immunostaining with primary antibodies for UFM1 (1:250, ab109305, Abcam), UFSP2 (1:100, sc-376084, Santa Cruz Biotechnology, Inc.), was performed overnight at 4°C, followed by incubation with Alexa Fluor® 647 conjugated anti-mouse IgG (1:500, A-21235, Invitrogen) and Alexa Fluor® 555 conjugated anti-rabbit IgG (1:1500, A-21428, Invitrogen) for 60 min at room temperature in the dark. Cell nuclei were stained with 4′, 6-diamidino-2-phenylindole (DAPI) (5 µg/mL) for 30 min at room temperature. After removing chambers from the slide, cells were mounted with Fluorescence Mounting Medium (DAKO) and analyzed by inverted confocal microscope Leica SP8X.

For tumor sphere immunofluorescence, 7.5×10^4 of Detroit 562 cells were cultured for 48 h in 24-well plates in a serum-free MEBM supplemented with B27, EGF and FGF, in order to form spheroids not larger than 200 µm. Cells were treated with 10 µg/mL poly(I: C) or poly(A: U) 24 h prior to immunostaining. After the treatment, spheres were fixed and permeabilized for 2 h at 4°C in PBS containing 4% formaldehyde and 1% Triton X-100. Spheres were than washed in PBS containing 0.1% Triton X-100 (PBST) and dehydrated in an ascending series of methanol diluted in PBS at 4°C (25%, 50%, 75/, 95% and 100%, 5 min each), followed by rehydration in the same descending series of methanols and washed in PBST. After blocking in PBST containing 5% Bovine Serum Albumin (BSA) for 30 min at room temperature, spheres were incubated overnight at 4°C with primary antibodies

CD133 (1:100, # MAB4399-I, Merck), UFM1 (1:250, ab109305, Abcam), UFSP2 (1:100, sc-376084, Santa Cruz Biotechnology, Inc.), and ALDH1 (1:100, sc-374076, Santa Cruz Biotechnology, Inc.). Subsequently, spheres were washed in PBST and incubated with Alexa Fluor® 647 conjugated anti-mouse IgG (1:500, A-21235, Invitrogen) and Alexa Fluor® 555 conjugated anti-rabbit IgG (1:1500, A-21428, Invitrogen) for 60 min at room temperature in the dark, followed by nuclear counterstaining with 4′, 6-diamidino-2-phenylindole (DAPI) (5 µg/mL) for 30 min at room temperature in the dark. After washing in PBST and centrifugation, spheroids were resuspended in 20 µl of supernatant and transferred onto a labelled slide, allowing spheroid suspension to settle. After carefully blotting the excess of buffer, spheroids were mounted with Fluorescence Mounting Medium (DAKO) and analyzed by inverted confocal microscope Leica SP8X.

Cytotoxicity assay

ViaLight Plus assay (Lonza Bioscience) was performed in order to determine the intracellular level of ATP, which is a measure of cell viability and reflects their metabolic function. The ViaLight Plus BioAssay was used according to the manufacturer's instructions. Briefly, cells were plated in 96-well low adhesion plates (FaCellitate, Germany) after the siRNA transfection. 48–72 h afterwards 50 µl of cell lysis reagent was added to each well and left for 75 min at room temperature to release ATP from cells, followed by ATP monitoring reagent. Luminescence was determined on a Tecan microplate reader at 1s integration.

RNA isolation and real time PCR

RNA was isolated with GenElute Mini Kit (Sigma-Aldrich, Germany), and 0.1 µg of RNA was used as a template for cDNA synthesis reaction by TaqMan ® Reverse Transcription Reagents Kit (Applied Biosystems, Branchburg, USA). The PCR reactions were performed with Sybr® Green PCR Master Mix (Applied Biosystems, Warrington, UK) on a QuantStudio 3 PCR Detection System (Applied Biosystems, USA) as described previously [8]. Primer sequences are: *ABCG2* F 5′-TACCTGTATAGT GTACTTCAT-3′, R 5′-GGTCATGAGAAGTGTTGCT A-3′; *CD133* F 5′-CAGAGTACAACGCCAAACCA-3′, R 5′-AAATCACGATGAGGGTCAGC-3′; UFM1-F 5′-GGC TGCCGTACAAAGTACTCA-3′, UFM1-R 5′-TTCCATC ATTGGTAATAATTGCAC-3′; UFC1-F 5′-TTTGGACT AGCTCATCTCATGG-3′, UFC1-R 5′-GAATCAGATCA GGGATTTCCAC-3′; UBA5-F 5′-CAGCACTGCCTAAA CAAGAGG-3′, UBA5-R 5′-TGAAACCTCAGATACCAG CTCA-3′; *28 S* F 5′-TTGAAAATCCGGGGGAGAG-3′, R 5′-ACATTGTTCCAACATGCCAG-3′.

Results

Proteomic and bioinformatic analysis revealed UFMylation pathway proteins as important players in tumor spheres

Initially, we aimed to determine if TLR3 has a role in HNSCC CSC maintenance, as it was shown in breast cancer [9], so we have analyzed proteomes of untreated adherent cells and the tumor spheres (untreated, treated with poly (I: C) and poly (A: U)) and determined there are 51 changed proteins in tumors spheres compared to adherent cells, 46 changed proteins in tumor spheres treated with poly (A: U) compared to untreated tumor spheres, and 22 changed proteins in poly (I: C)-treated tumor spheres compared to the untreated tumor spheres. By using STRING analysis, we have determined many different protein interactions (Fig. 1). However, in this paper we have decided to focus on the UFMylation pathway, as several of the changed proteins belonged to this pathway: UFSP2 and DDRGK1 as enzymes involved in this system, and RPL9 and RPL29 as target proteins of UFMylation. UFSP2 and DDRGK1 were shown in the proteomic analysis as downregulated after poly (A: U) stimulation of spheres when compared to untreated spheres (fold change 0.4 and 0.3, respectively), and RPL9 and RPL29 were shown as upregulated in control spheres (fold change 2.25 and 2.0, respectively) when compared to adherent cells (Supplementary Table 1). Figure 2 shows diagrams of different biological processes (Fig. 2a), and protein classes (Fig. 2b) that are changed after comparison of untreated tumor spheres to adherent cells, and after comparison of poly (I: C) and poly (A: U) treated tumor spheres and untreated spheres. Figure 2c shows volcano plots showing distribution of the up-regulated (green) and down-regulated (red) proteins after the comparison of untreated tumor spheres to adherent cells, and after the comparison of poly (I: C) and poly (A: U) treated tumor spheres and untreated spheres. Figure 2d shows Venn diagram of common proteins across examined groups.

Western blot confirmed the increased expression of UFMylation pathway proteins in tumor spheres compared to adherent cells

First, we sought to confirm the proteomic results by western blot. We obtained similar results and found that UFSP2 and DDRGK1 were downregulated in tumor spheres treated with poly (A: U) in comparison to untreated spheres. Unexpectedly, we found that both of these proteins were upregulated in untreated tumor spheres in comparison to adherent cells. In adherent cells, these proteins were faintly expressed, and there was no difference in their expression between the control adherent cells and treated adherent cells (either with poly(I: C) or poly (A: U)) (Fig. 3a). In addition, comparable results were observed with other proteins of the

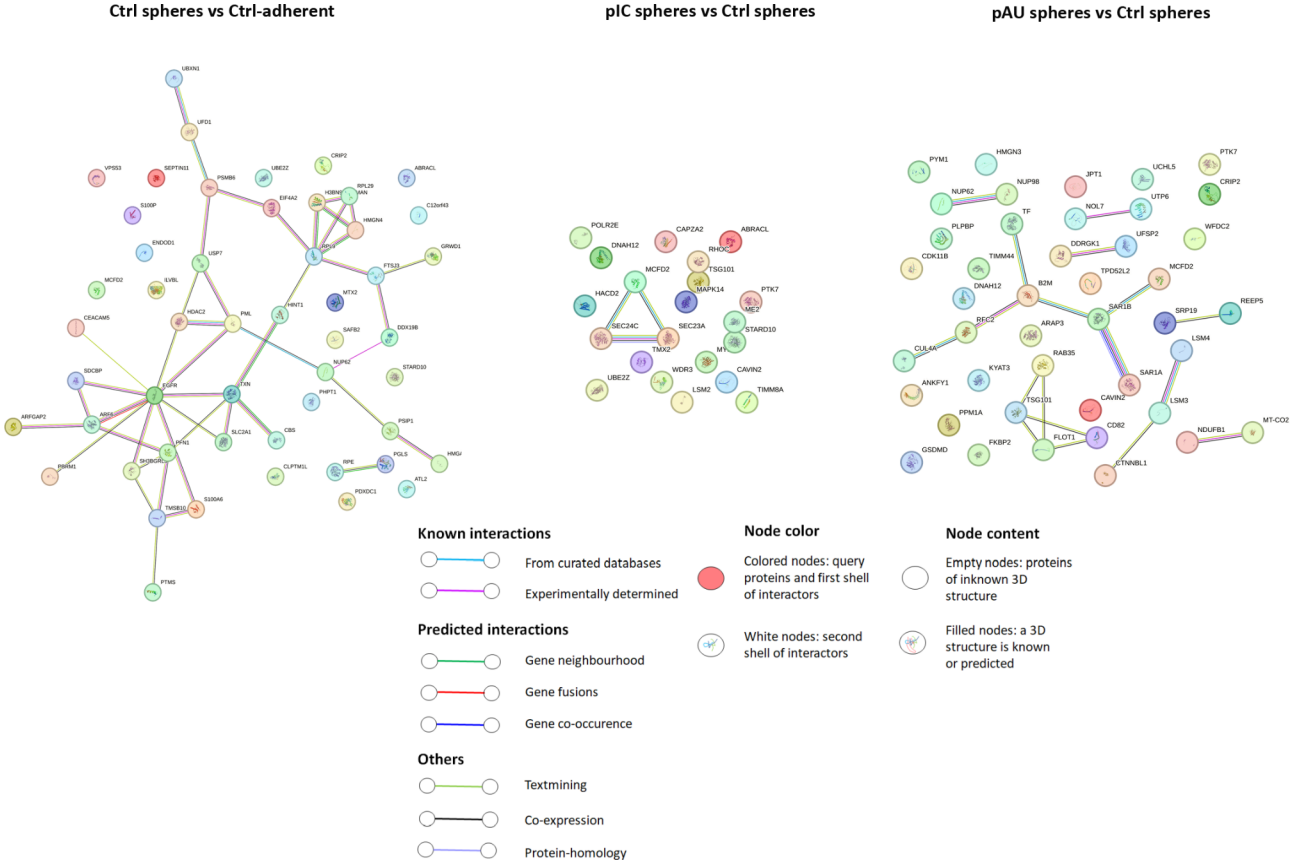

Fig. 1 STRING diagrams of protein interactions of altered proteins. We have compared untreated spheres (Ctrl spheres) to untreated adherent cells (Ctrl-adherent), spheres treated with poly (I: C) (pIC spheres) compared to untreated spheres (Ctrl spheres) and spheres treated with poly (A: U) (pAU spheres) compared to untreated spheres (Ctrl spheres)

UFMylation system, UFL1 and DDRGK1, which were also upregulated in tumor spheres and downregulated after the treatment with poly (A: U) (Fig. 3b). The treatment of adherent cells with poly (I: C), and poly (A: U) did not affect UFL1 expression, but poly (A: U) treatment did reduce DDRGK1 expression. We have also confirmed UFSP2 expression results in another pharyngeal cancer cell line, FaDu cells, that were transfected with shTLR3 induced by doxycycline. Additionally, we have corroborated this in Detroit 562 cells, transiently transfected with TLR3 siRNA (Fig. 3c).

Finally, by immunocytochemistry, we have confirmed that UFSP2 is strongly expressed in tumor spheres, but not in adherent cells, which was also statistically significant. The UFSP2 showed mainly cytoplasmic localization. Also, we have demonstrated that tumor spheres treated with poly (A: U) show lower expression of UFSP2 than untreated spheres (Fig. 3d). Moreover, we have confirmed by immunocytochemistry that poly(A: U) treatment of tumor spheres also reduces UFSP2 expression (Fig. 3e). Since there was such a dramatic increase in the expression of UFMylation pathway proteins (UFSP2, DDRGK1, and UFL1) in CSCs compared to their adherent controls, we pursued this phenomenon further to reveal the role of UFMylation in CSCs and focused solely on the role of UFMylation in CSCs.

UFM1 is upregulated in HNSCC, and its high expression is connected with poor survival and EMT

Subsequently, we have performed a bioinformatic analysis of UFMylation pathway genes (UFM1, DDRGK1, UFL1, and UFSP2) and demonstrated that among the tested proteins, only UFM1 was highly expressed in HNSCC compared to the normal tissue, and that high UFM1 expression was associated with poor overall survival and disease-free survival in HNSCC patients (Fig. 4a and b, and Fig. 1 Supplementary data). We have also shown that UFM1 is positively correlated with several key genes involved in the EMT (ZEB1, TWIST1, and FN1) in HNSCC tumor samples, but not in normal samples (Fig. 4c), suggesting they might have a role in cancer progression [20, 21]. Additionally, we found positive UFL1/ZEB1 correlation in HNSCC tumor samples but not in normal (Fig. 1 Supplementary data). The results were calculated using the online web service GEPIA (http://gepia.cancer-pku.cn/index.html). Therefore,

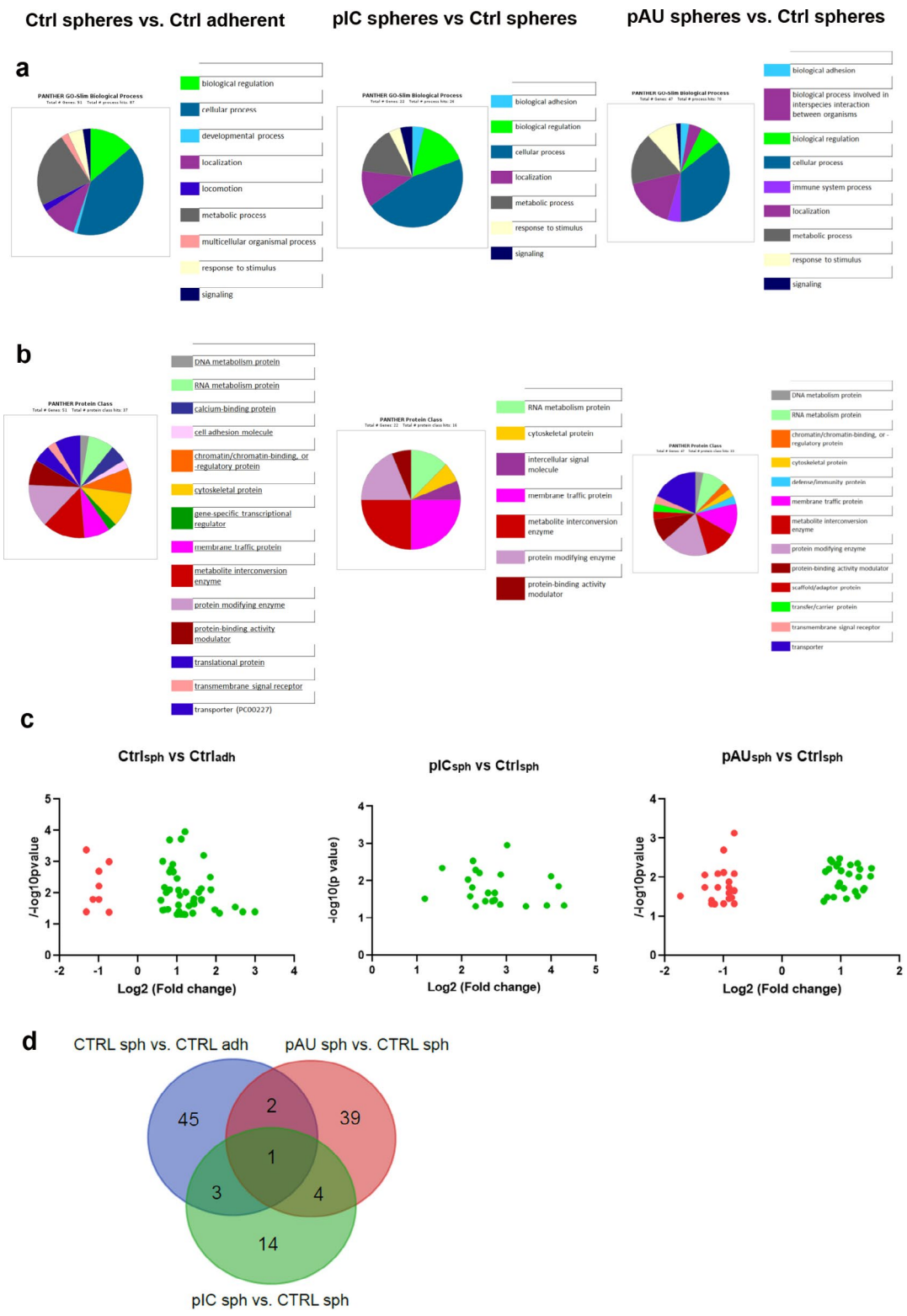

Fig. 2 Diagrams of different biological processes (Fig. 2a), and protein classes (Fig. 2b) that are changed after comparison of untreated tumor spheres to adherent cells, and after comparison of poly (I: C) and poly (A: U) treated tumor spheres and untreated spheres. Volcano plots showing distribution of the up-regulated (green) and down-regulated (red) proteins after the comparison of untreated tumor spheres to adherent cells, and after the comparison of poly (I: C) and poly (A: U) treated tumor spheres and untreated spheres (Fig. 2c). Figure 2d shows Venn diagram of common proteins across examined groups

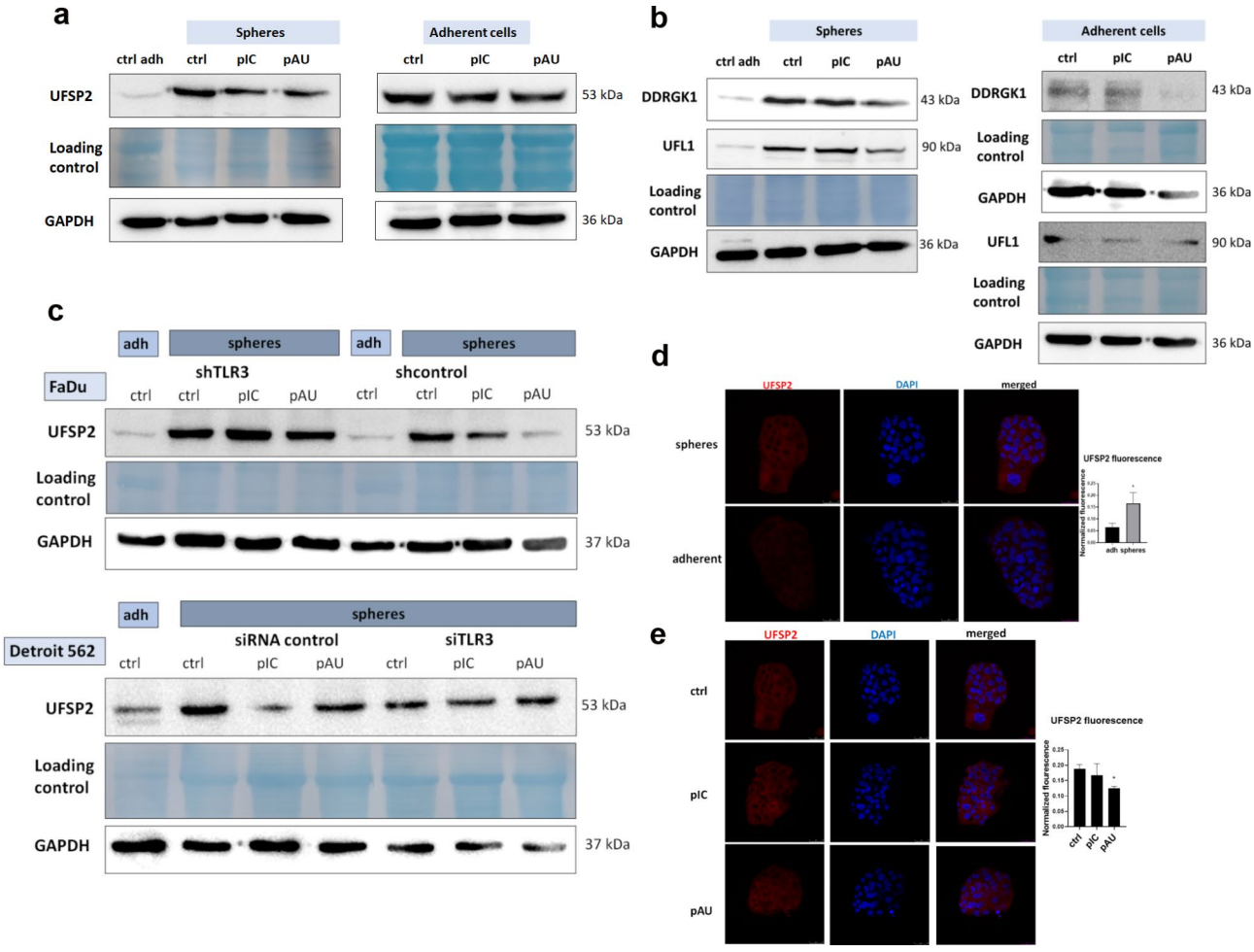

Fig. 3 The expression of the UFMylation system proteins. We have compared the untreated tumor spheres or tumor spheres treated with poly (I: C) or poly (A: U). UFSP2 expression in Detroit 562 spheres and adherent cells after the treatment with poly (I: C) or poly (A: U) (Fig. 3a). UFSP2 expression in FaDu cells transfected with inducible shRNA for TLR3 treated with poly (I: C) or poly (A: U), and in Detroit 562 cells after transient transfection with TLR3 siRNA and treatment with poly (I: C) or poly (A: U) (Fig. 3b). UFSP2 expression by immunocytochemistry in Detroit 562 adherent cells and tumor spheres (Fig. 3c). DDRGK1 and UFL1 expression in Detroit 562 control adherent cells or tumor spheres after the treatment with poly (I: C) or poly (A: U) (Fig. 3d).* $p > 0.05$ (compared to adherent cells). UFSP2 expression by immunocytochemistry in Detroit 562 untreated tumor spheres, and spheres treated with poly (I: C), and poly (A: U) (Fig. 3e)

we hypothesized that UFM1 might have a role in CSCs maintenance and HNSCC progression.

UFM1 is strongly expressed in tumor spheres compared to the adherent cells, and UFM1 silencing reduces the number and size of tumor spheres and stemness

We have shown next that UFM1 is strongly upregulated in tumor spheres of Detroit 562 cells, in comparison to the adherent Detroit 562 cells. Its localization was mainly cytoplasmic. Interestingly, poly(I: C)-treated adherent cells showed the aggregation of UFM1 in some sort of vesicles. However, even though in adherent cells there was no difference in the UFM1 expression between the control cells and those treated with TLR3 agonists poly (I: C) and poly (A: U), in control tumor spheres the difference in its expression was astonishing. In tumor spheres treated with poly (I: C) and poly (A: U) UFM1 was even less expressed than in control adherent cells (Fig. 5a).

UFM1 siRNA transfection of Detroit 562 cells reduced sphere number and size (Fig. 5b). We have compared the spheres transfected with control siRNA and spheres transfected with siRNA for UFM1 gene in 2 systems: 96 well with only 3×10^3 cells seeded which made one large sphere and in 24 well plates where 7.5×10^4 cells were seeded and made multiple spheres. In both systems siUFM1-transfected cells made smaller spheres, where fewer of them were in size between 200 µm and 350 µm. Moreover, UFM1 silencing (Fig. 5c) reduced the survival of tumor spheres (Fig. 5d). By qPCR and western blot, we have confirmed that UFM1 is silenced (Fig. 5c), and that CD133 expression is significantly decreased (up to 50%). Oct4 was moderately decreased in siUFM1 cells while

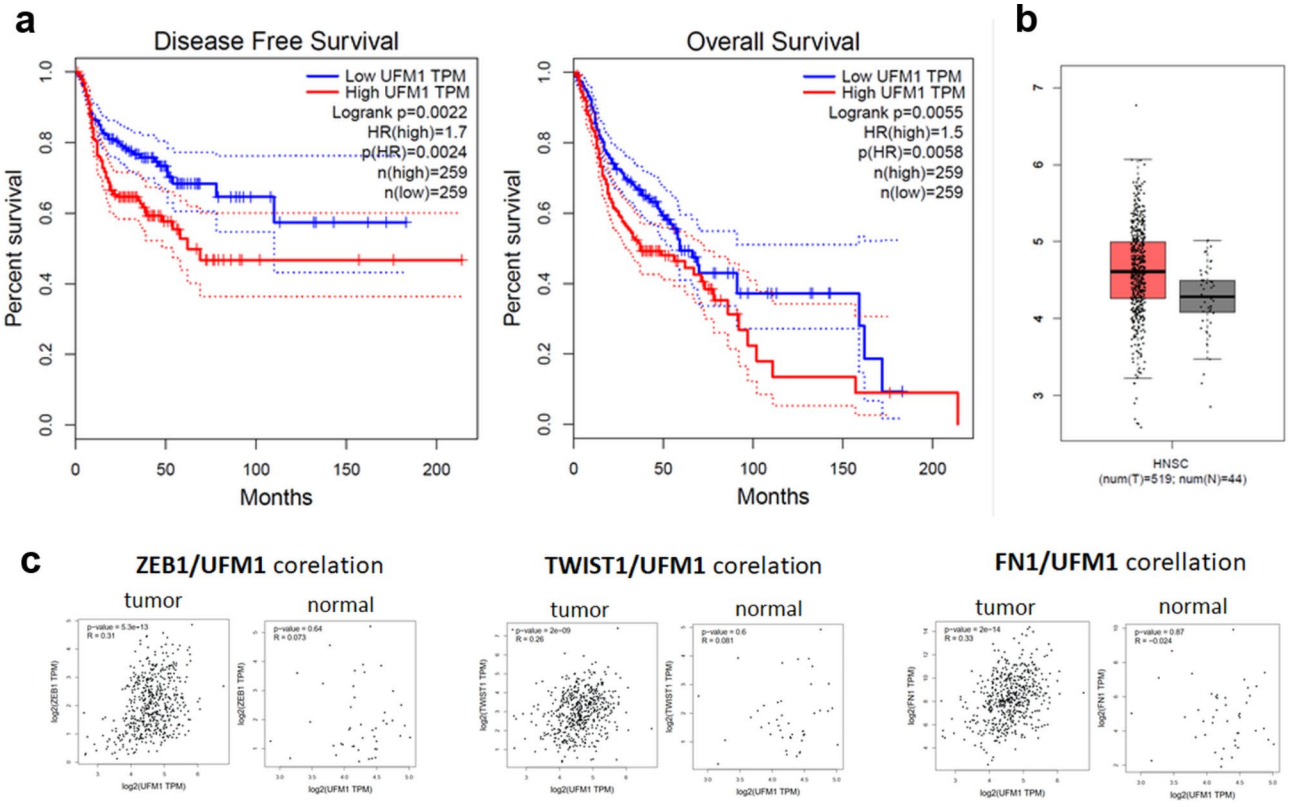

Fig. 4 High UFM1 expression predicts worse prognosis in HNSCC patients. Disease free survival and overall survival depending on UFM1 expression in HNSCC (Fig. 4a), and the expression of UFM1 in HNSCCC compared to normal (Fig. 4b). Correlation of UFM1 with ZEB1, TWIST1 and fibronectin in HNSCC compared to normal tissue (Fig. 4c). All figures were made by GEPIA

ABCG2 was reduced by almost 50%. EMT genes, fibronectin and vimentin, were significantly decreased up to 60% and 40%, respectively (Fig. 5e). Immunocytochemistry showed that UFM1 silencing dramatically reduces CD133 expression, and moderately reduces ALDH1 expression in tumor spheres in a statistically significant manner (Fig. 5f). We have also proved the co-localization of CD133 and ALDH1 with UFM1 in untreated tumor spheres (Fig. 5g).

Mithramycin reduces tumor sphere formation and induces apoptosis by targeting transcription factor Sp1

Our bioinformatic analysis of transcription factors involved in the regulation of proteins which were altered in proteomic analysis, performed by Funrich, revealed that Sp1 controls the expression of almost 50% of altered genes/proteins (Fig. 6a). Therefore, we wanted to see if mithramycin (MTH), an Sp1 inhibitor [22–24], could be effective in eradicating CSCs. MTH also inhibits EMT in salivary cystic adenocarcinoma [25], and in breast cancer [26]. Hence, we have treated tumor spheres with different concentrations of MTH and revealed that after 72 h of treatment, even the lowest concentration used effectively destroys the tumor spheres. The cells appeared dead and were weakly connected within the tumor spheres, which was most obvious at the highest concentration where almost no spheres were left. Also, after 48 h of treatment, 100 nM and 200 nM concentrations of MTH showed more individual cells between spheres, suggesting that some spheres have started to disrupt, while spheres treated with 50 nM of MTH looked similar to the control ones (Fig. 6b). Furthermore, the expression of CD133 expression was markedly reduced following a 24-hour treatment with 100 nM MTH (Fig. 6c). In MTH-treated spheres after 48 h, we observed PARP cleavage even with the treatment with 50 nM MTH uncovering the mechanism of cell death as apoptosis. Western blot analysis of Sp1 expression revealed no Sp1 was detected in MTH-treated cells 48 h after the treatment with 100 and 200 nM MTH, and residual traces of Sp1 expression in the cells treated with 50 nM MTH (Fig. 6d). The UFMylation process was disrupted in MTH-treated tumor spheres after 48 h with 50 and 100 nM concentrations, as both UFM1 and UFM1 conjugates were weakly expressed compared to the control cells. Moreover, after 72 h, there is almost no visible UFM1 and UFM1 conjugates expression (Fig. 6e).

MTH showed significant cell toxicity of tumor spheres treated with 50 nM, 100 nM, and 200 nM concentrations for 48 and 72 h. The survival of Detroit 562 tumor

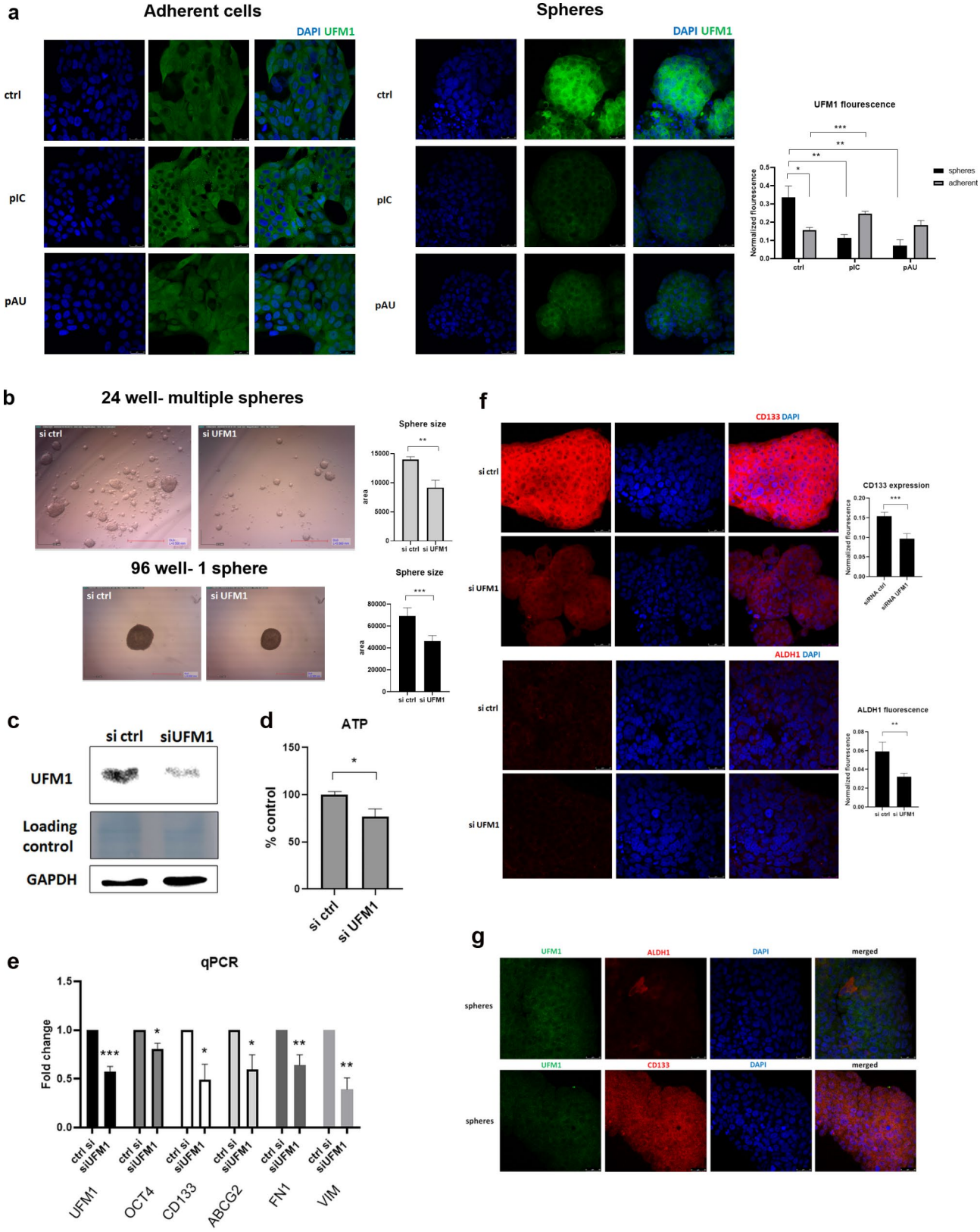

Fig. 5 (See legend on next page.)

(See figure on previous page.)

Fig. 5 The UFM1 expression is increased in tumor spheres and associated with their size and stemness. The expression and colocalization of UFM1 in adherent cells and tumor spheres treated with poly (I: C) or poly (A: U); * $p > 0.05$, ** $p > 0.03$, ** $p > 0.01$ (compared to adherent cells) (Fig. 5a). Tumor spheres size in cells transfected with control siRNA and those transfected with UFM1 siRNA; * $p > 0{,}05$, ** $p > 0{,}01$, *** $p > 0{,}005$ (compared to control siRNA) (Fig. 5b). The expression of UFM1 after the siRNA silencing shown by western blot (Fig. 5c). The survival of UFM1-silenced tumor spheres (Fig. 5d). The expression of UFM1, OCT4, CD133, ABCG2, fibronectin, and vimentin after UFM1 silencing shown by qPCR; * $p > 0.05$, ** $p > 0.03$, *** $p > 0.01$, **** $p > 0{,}001$ (compared to control siRNA) (Fig. 5e). Immunocytochemistry shows reduced expression of CD133 and ALDH1 after UFM1 silencing; * $p > 0.05$, ** $p > 0.03$, *** $p > 0.005$ (compared to control siRNA) (Fig. 5f). Co-localization of CD133 and ALDH1 with UFM1 in untreated tumor spheres (Fig. 5g)

spheres was reduced almost to half after 48 h of 50 nM MTH treatment, and even to 30% after 48 h of treatment with 200 nM MTH. After 72 h of treatment, all concentrations showed less than 30% survival. To test whether this therapy could be effective in other HNSCC lines, we included FaDu, another pharyngeal cancer cell line, and Cal 27, tongue adenosquamous carcinoma cell line. FaDu cells were the most sensitive as even the lowest concentration used (50 nM) induced 90% cell death after only 48 h, and the survival was reduced to 5% after 72 h of treatment with all concentrations used. Cal 27 appeared to be more resilient than FaDu in terms of cell survival, as after 48 h of treatment the survival was reduced to 40–50%, and after 72 h it was even lower than 40%. However, their tumor spheres were the only spheres that appeared disrupted after the treatment, as some accumulation of cells was visible around the spheres (Fig. 6f).

Also, DDRKG1, a protein belonging to the UFMylation system was downregulated after 24 h following 100 and 200 nM MTH treatment, while UFSP2 and UFL1 were not affected, as we have shown by western blot (Fig. 6g). By qPCR, we have shown that MTH treatment reduced the expression of other two important genes from the UFMylation system: UBA5 and UFC1 (Fig. 6h). Moreover, we have revealed that MTH treatment, besides inhibiting the expression of stemness genes OCT4, CD133, and ABCG2, also targets the expression of the principal UFMylation target RPL26 [14]. It did not seem to affect RPL9 and TLR3 expression.

Discussion

Our data show that HNSCC CSCs express high levels of UFMylation system proteins (UFSP2, DDRGK1, and UFM1). By exploring the UFM1 role in CSCs we showed that its high expression significantly influences disease-free and overall survival, as well as that its expression is corelated with several EMT genes. By UFM1 siRNA inhibition we decreased the stemness and the maintenance of CSCs. By targeting Sp1 with mithramycin, we indirectly targeted UFM1 and also reduced the survival, and stemness and induced the apoptosis of CSCs. To our knowledge, this is the first study on the role of UFMylation in CSCs.

The role of UFMylation in cancer is still unknown. Some studies indicate its cancer-suppressive role, for example in UFMylation of p53 which stabilizes p53 by preventing MDM2-mediated ubiquitination [13], while others suggest it has a role in tumor development [16, 27]. It has been reported that UFM1 is strongly expressed in the cancer tissue compared to the normal adjacent tissue [28], however, in gastric cancer the opposite was observed [29]. A very recent study, and this is the only one linking UFM1 and HNSCC, demonstrated that elevated UFM1 expression was associated with poor prognosis and immune infiltration in OSCC, while the inhibition of UFM1 expression delayed OSCC progression by inhibiting cell proliferation, migration, and invasion [30]. It is also important to emphasize that to date, only a few direct UFMylation substrates have been identified, including UFBP [31], RPL26 [14], RPN1 [32], ASC1 [27], p53 [13], Histon H4 [11], PLAC8 [33], MRE11 [34], and CYB5R310 [35].

Only a few publications and just two clinical studies (according to clinicaltrials.gov; NCT01624090 and NCT02859415) have reported the inhibitory effect of MTH on the CSCs. More than 10 years ago, Zhang and colleagues reported that cigarette smoke induces ABCG2 as a result of Sp1 binding to its promoter in lung and esophageal cancer. Mithramycin treatment not only downregulated ABCG2 but microarray analysis also revealed that it targeted multiple stem cell-related pathways [36]. In colon cancer, it was demonstrated that the inhibition of Sp1 by mithramycin suppresses CSC growth and induces apoptosis in vitro and in vivo [37, 38]. Therapy-resistant breast cancer CSCs can be sensitized to doxorubicin by MTH [39]. As a potential CSC therapy, MTH was also explored in sarcoma [40], glioblastoma [41], and non-small cell lung cancer cells [42]. Since MTH has high toxicity in humans exhibiting adverse manifestations in multiple organs/ cell systems [43], genetical engineering of its biosynthetic pathway resulted in different mithramycin analogs (mithralogs) with improved pharmacological and toxicological properties [44, 45]. A leading mithralog is EC-8042, which is 10 times less toxic than mithramycin while also showing strong antitumor activity, also against CSCs in prostate cancer [46] sarcoma [40], and head and neck cancer [47]. The latter publication demonstrated the efficacy of EC-8042 against CSCs in vivo in a FaDu xenograft model, thus the authors concluded this mithralog should be clinically tested in HNSCC patients. This is also the only study involving the successful treatment of HNSCC CSCs by mithralog. Another interesting study showed that a combination therapy involving mithramycin and checkpoint blockade

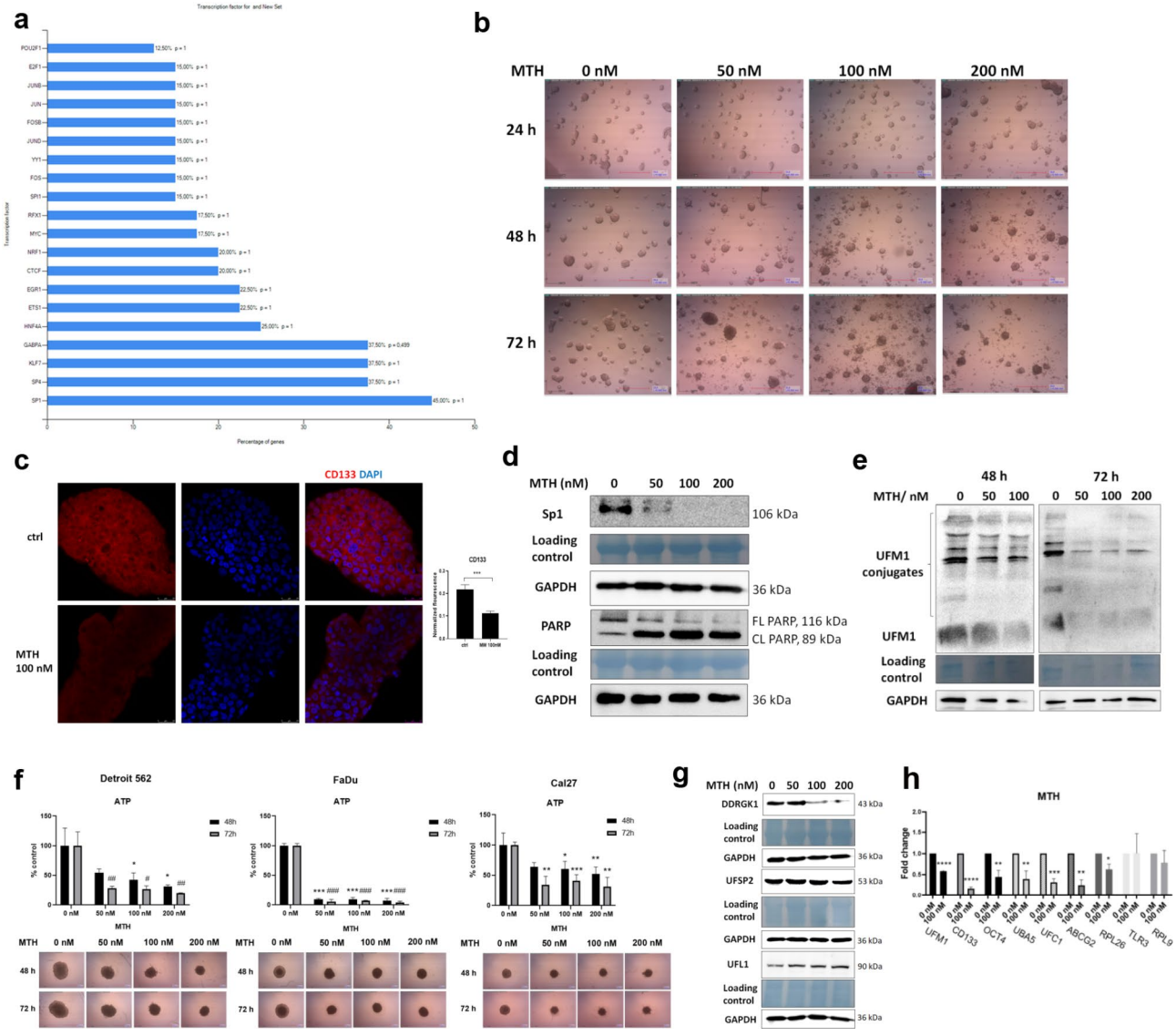

Fig. 6 Mithramycin inhibits tumor sphere formation by targeting Sp1 transcription factor. Funrich graphs demonstrate Sp1 as the main transcription factor of almost half of the altered proteins between the tumor spheres and adherent cells (Fig. 6a). MTH reduced tumor sphere number and size after 72 h of treatment (Fig. 6b), and CD133 expression after 24 h of treatment; * $p > 0.05$, ** $p > 0.03$, *** $p > 0.01$ (compared to untreated cells) (Fig. 6c). MTH reduced Sp1 expression and induced apoptosis by increasing the expression of cleaved PARP variant, as shown by the western blot (Fig. 6d). MTH reduced UFM1 expression as well as the expression of UFM1-conjugates (Fig. 6e). MTH reduced the survival of Detroit 562, FaDu, and Cal27 tumor spheres; * $p > 0.05$, ** $p > 0.03$, *** $p > 0.005$, # $p > 0.05$, ## $p > 0.03$, ### $p > 0.005$ (*represents the statistical significance compared to the untreated cells, and after 48 h, and # represents the statistical significance to the untreated cells after 72 h) (Fig. 6f). MTH reduced the expression of DDRGK1, but not UFSP2 or UFL1 (Fig. 6g). MTH reduced expression of UFM1, CD133, OCT4, UBA5, UFC1, ABCG2, RPL26, TLR3, and RPL9; * $p > 0.05$, ** $p > 0.03$, *** $p > 0.01$, **** $p > 0.001$ (compared to the untreated cells) (Fig. 6h)

decreases tumor growth and increases CD8+T cell infiltration while diminishing immunosuppression, thus revealing this drug combination could be used in immunologically cold tumors [48]. Moreover, mithramycin systemic toxicity can be reduced by its encapsulation in nano-delivery systems as explored recently [49]. Other potential Sp1 inhibitors with less toxicity but Sp1 inhibitory action should also be explored, including berberine, which has been shown to sensitize nasopharyngeal carcinoma cells to radiation [50].

Even though it has been shown that UFMylation stabilizes p53 as shown in HeLa, HCT116, and U2OS which have wild type p53 [13], in the case of cells lines with mutant p53 which were used in our study (Detroit 562- p.R175H, FaDu- p.R248L, and Cal27- p.H193L), the mechanism might be different. Also, these authors showed that depletion of UFL1 or DDRGK1 decreases p53 stability and in turn, promotes cell growth and tumor formation in vivo. However, we have shown here that these proteins are overexpressed in CSCs. Additionally,

these authors checked UFL1 and DDRGK1 expression only on renal cell carcinomas and determined that these proteins are highly expressed in adjacent normal tissue but poorly expressed or even absent in cancer tissue. In HNSCC, as previously mentioned, Ke et al. revealed that high UFM1 overexpression was associated with short overall survival, disease-specific survival, and progression-free interval, and was an adverse factor for prognosis in OSCC. However, these authors only used bioinformatic analysis using data from OSCC patients from The Cancer Genome Atlas (TCGA) database. Consequently, the role of UFMylation in p53 mutant tumors, especially the patients' cancerous tissue, should be further investigated.

It is important to highlight that recent studies show that expression levels of UFMylation machinery is tightly regulated to maintain proper system functioning, and any deviation from this could affect critical cellular functions, including migration, proliferation and stemness. For example, it has been shown that that overexpression of UBA5 enzyme has inhibiting effect on UFMylation process similar to the deletion of UBA5, which subsequently resulted in significantly reduced ability of cells to migrate [51]. Moreover, a study by Wang et al. has shown that overexpression of UFSP2 in pancreatic adenocarcinoma cell lines (PANC-1 and Mia PaCa-2 cells) interferes with UFMylation of RPL10 and not only reduces the proliferation and colony formation ability, but also leads to decreased size and the expression of stemness markers in spheres [28].The immune system also dictates tumor fate, as a higher immune response is significantly associated with better clinical outcomes. Few recent studies show a connection between UFMylation and the immune system response indicating the importance of this modifications not only in the malignant tissue but also in the immune reaction. However, the role of UFMylation in immune system control is still not clear, and the number of studies is limited. One study suggests that PDL1 UFMylation promotes its proteasome-mediated degradation and that reduced UFMylation of this protein leads to immune evasion [52]. Conversely, the other study demonstrated that UFMylation of PLAC8, a candidate oncogene, maintains its stability, and that high PLAC8 expression in triple-negative breast cancer (TNBC) cells promotes cell proliferation and inhibits T lymphocyte activity by upregulating PD- L1 expression [33] suggesting that reduced UFMylation should improve therapeutical benefits. UFMylation also inhibits the proinflammatory capacity of interferon-γ (IFN-γ) -activated macrophages (MFs) [53]. The authors demonstrated recently that the UFMylation pathway suppresses responses to both IFN-γ and LPS and reduces transcripts of their target genes suggesting that this pathway may have a key role in both innate and adaptive immunity. Negative regulation of IFN-γ and LPS-mediated macrophage activation required the enzymatic activity of Ufsp2, Uba5, and Ufc1. Since type 1 MFs are activated mainly by LPS and IFN-γ, this way their activation is stopped. If this can happen in the tumor microenvironment, it is possible that with this type of UFMylation-based control, the activation of M2 type macrophages, well-known for their pro-tumorigenic role, may prevail. We can speculate whether CSCs might highjack this system of negative regulation by UFMylation to skew the M1/M2 balance towards pro-tumorigenic M2 phenotype, which ultimately might ensure the tumor-permissive microenvironment that supports immunosuppression and cancer progression. Similarly, Song et al. recently showed that tumor-derived UBR5 (Ubiquitin E3 ligase) not only affects tumor-associated macrophages (TAMs) recruitment to TME in a paracrine manner but also TAMs' immunosuppressive activity [54]. It would be interesting to see if the UFMylation system proteins derived from HNSCC CSCs might have the same effect on the macrophages in the tumor microenvironment. To sum up, all these data suggest CSCs might use UFMylation for immune system evasion, and more research is needed in this direction.

We have shown here that MTH diminishes the expression of DDRGK1, as well as the expression of ABCG2, the marker of chemoresistance. Wang et al. recently showed that DDRGK1 enhances osteosarcoma chemoresistance via inhibiting KEAP1-mediated NRF2 ubiquitination [55], so this might be the mechanism by which MTH can reduce chemoresistance in our model providing another convincing argument for MTH therapy of CSCs. We have also demonstrated that MTH treatment influences the expression of more than half of the UFMylation system proteins. It is important to emphasize that if certain proteins of the UFMylation system are absent, such as in our case DDRGK1, UBA5, and UFC1, the UFM1 also cannot be transferred, and UFMylation of the target genes will be reduced. More specifically, DDRGK1 is an adaptor protein for UFL1, anchored at the ER, and forms a scaffold-type ligase complex with UFL1, thus binding to UFC1 to promote aminolysis and transfer UFM1 onto substrates. Therefore, we have shown here that MTH treatment downregulates two crucial proteins from the final complex which transfers UFM1 to the substrate, which suggests that MTH can reduce UFMylation in CSCs, induce apoptosis, and reduce chemoresistance, leading to successful therapy. While our study provides valuable insights, it is important to acknowledge that a considerable limitation of our study is the lack of an CSC xenograft model which would be valuable to confirm that UFMylation phenotype is closely related to the CSC stemness. Following studies involving in vivo experiments will allow us to better understand the underlying

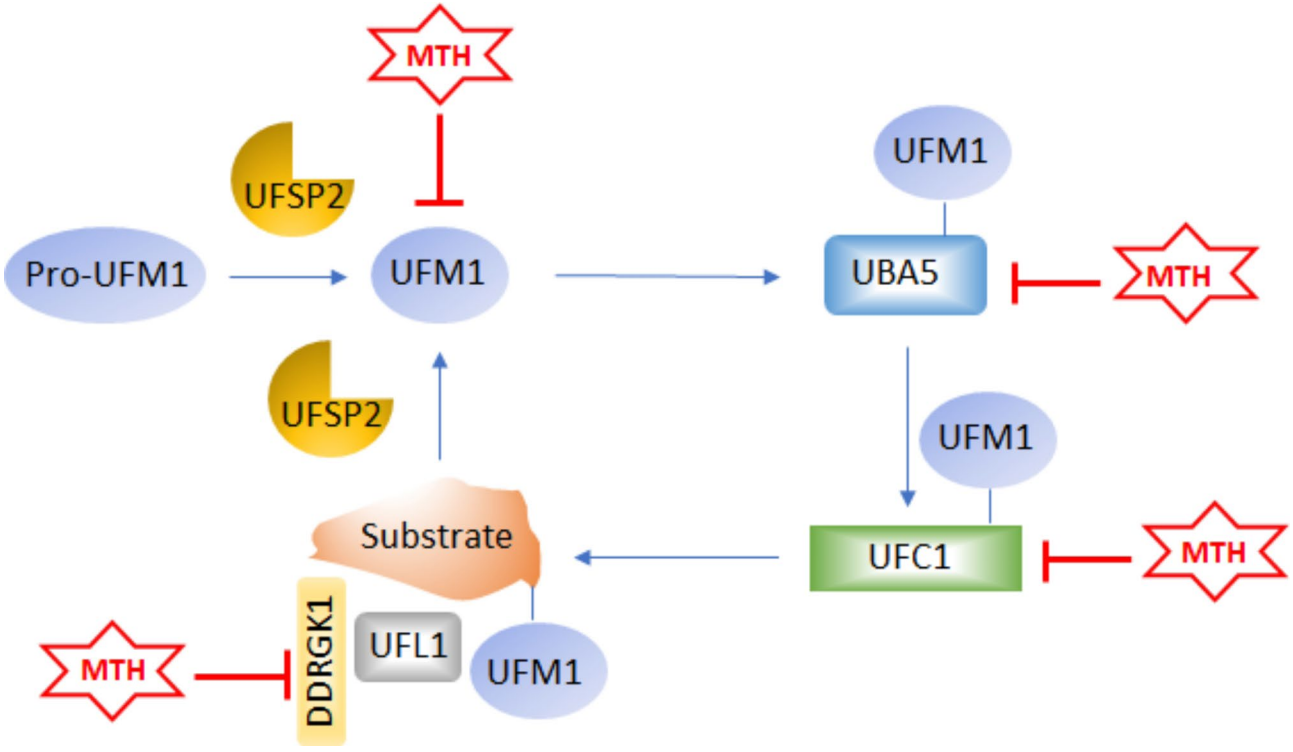

Fig. 7 MTH downregulates most of the UFMylation system proteins (UFM1, UBA5, UFC1, and DDRGK1) in HNSCC CSCs

mechanism and assess the physiological relevance as well as therapeutic implications of our findings.

Conclusion

We conclude herein that UFMylation has an important role in HNSCC CSCs while the inhibition of UFM1 or other proteins of the UFMylation system such as DDRGK1, UBA5, or UFC1, could delay HNSCC progression by acting upon CSCs (Fig. 7). This inhibition can be achieved by Sp1 inhibitors mithramycin or its analogs. Our results indicate that UFM1 could become a prognostic biomarker and a therapeutic target for HNSCC with special emphasis in the eradication of CSCs through the induction of apoptosis.

Supplementary Information

The online version contains supplementary material available at https://doi.org/10.1186/s12935-024-03609-6.

Supplementary Material 1

Supplementary Material 2

Author contributions

K.V.D. performed most of the experiments, analyzed data, and edited the manuscript. T.V. performed the experiments, and also revision experiments. T.D. performed the experiments. T.M.G. designed the study content, analyzed data, produced figures, wrote the first draft, secured resources, supervised the study, and wrote the final version of the manuscript. All authors read and approved the finals version of the manuscript.

Funding

This work was supported by Croatian Science Foundation (project number: IP-2020-02-4225 Toll-like receptor 3 in the development and treatment of human head and neck cancer: the role of endogenous ligands) and Young Researchers' career development project- training of doctoral students (Croatian Science foundation).

Data availability

No datasets were generated or analysed during the current study.

Declarations

Ethics approval and consent to participate

Not applicable.

Competing interests

The authors declare no competing interests.

Received: 5 July 2024 / Accepted: 10 December 2024
Published online: 19 December 2024

References

1. Derfi KV, Vasiljevic T, Glavan TM. Recent Advances in the Targeting of Head and Neck Cancer Stem Cells. Appl Sci-Basel.2023;13.
2. Vasiljevic T, Tarle M, Hat K et al. Necrotic Cells from Head and Neck Carcinomas Release Biomolecules That Are Activating Toll-like Receptor 3. Int J Mol Sci.2023;24.
3. Kariko K, Ni H, Capodici J, et al. mRNA is an endogenous ligand for Toll-like receptor 3. J Biol Chem. 2004;279:12542–50.
4. Salaun B, Coste I, Rissoan MC, et al. TLR3 can directly trigger apoptosis in human cancer cells. J Immunol. 2006;176:4894–901.
5. Matijevic Glavan T, Cipak Gasparovic A, Verillaud B, et al. Toll-like receptor 3 stimulation triggers metabolic reprogramming in pharyngeal cancer cell line through Myc, MAPK, and HIF. Mol Carcinog. 2017;56:1214–26.

6. Veyrat M, Durand S, Classe M, et al. Stimulation of the toll-like receptor 3 promotes metabolic reprogramming in head and neck carcinoma cells. Oncotarget. 2016;7:82580–93.
7. Paone A, Galli R, Gabellini C, et al. Toll-like receptor 3 regulates angiogenesis and apoptosis in prostate cancer cell lines through hypoxia-inducible factor 1 alpha. Neoplasia. 2010;12:539–49.
8. Matijevic T, Pavelic J. The dual role of TLR3 in metastatic cell line. Clin Exp Metastasis. 2011;28:701–12.
9. Jia D, Yang W, Li L, et al. beta-Catenin and NF-kappaB co-activation triggered by TLR3 stimulation facilitates stem cell-like phenotypes in breast cancer. Cell Death Differ. 2015;22:298–310.
10. Millrine D, Peter JJ, Kulathu Y. A guide to UFMylation, an emerging posttranslational modification. FEBS J. 2023;290:5040–56.
11. Qin B, Yu J, Nowsheen S, et al. UFL1 promotes histone H4 ufmylation and ATM activation. Nat Commun. 2019;10:1242.
12. Lemaire K, Moura RF, Granvik M, et al. Ubiquitin fold modifier 1 (UFM1) and its target UFBP1 protect pancreatic beta cells from ER stress-induced apoptosis. PLoS ONE. 2011;6:e18517.
13. Liu J, Guan D, Dong M, et al. UFMylation maintains tumour suppressor p53 stability by antagonizing its ubiquitination. Nat Cell Biol. 2020;22:1056–63.
14. Walczak CP, Leto DE, Zhang L, et al. Ribosomal protein RPL26 is the principal target of UFMylation. Proc Natl Acad Sci U S A. 2019;116:1299–308.
15. Wei Y, Xu X, UFMylation:. A Unique & Fashionable Modification for Life. Genomics Proteom Bioinf. 2016;14:140–46.
16. Yoo HM, Park JH, Kim JY, et al. Modification of ERalpha by UFM1 Increases Its Stability and Transactivity for Breast Cancer Development. Mol Cells. 2022;45:425–34.
17. Wang K, Chen S, Wu Y, et al. The ufmylation modification of ribosomal protein L10 in the development of pancreatic adenocarcinoma. Cell Death Dis. 2023;14:350.
18. Yang J, Zhou Y, Xie S, et al. Metformin induces Ferroptosis by inhibiting UFMylation of SLC7A11 in breast cancer. J Exp Clin Cancer Res. 2021;40:206.
19. Hu Z, Wang X, Li D, et al. UFBP1, a key component in ufmylation, enhances drug sensitivity by promoting proteasomal degradation of oxidative stress-response transcription factor Nrf2. Oncogene. 2021;40:647–62.
20. Major AG, Pitty LP, Farah CS. Cancer stem cell markers in head and neck squamous cell carcinoma. Stem Cells Int. 2013;2013:319489.
21. Yu SS, Cirillo N. The molecular markers of cancer stem cells in head and neck tumors. J Cell Physiol. 2020;235:65–73.
22. Choi ES, Nam JS, Jung JY, et al. Modulation of specificity protein 1 by mithramycin A as a novel therapeutic strategy for cervical cancer. Sci Rep. 2014;4:7162.
23. Blume SW, Snyder RC, Ray R, et al. Mithramycin inhibits SP1 binding and selectively inhibits transcriptional activity of the dihydrofolate reductase gene in vitro and in vivo. J Clin Invest. 1991;88:1613–21.
24. Seznec J, Silkenstedt B, Naumann U. Therapeutic effects of the Sp1 inhibitor mithramycin A in glioblastoma. J Neurooncol. 2011;101:365–77.
25. Li J, Gao H, Meng L, et al. Mithramycin inhibits epithelial-to-mesenchymal transition and invasion by downregulating SP1 and SNAI1 in salivary adenoid cystic carcinoma. Tumour Biol. 2017;39:1010428317708697.
26. Kwon YJ, Baek HS, Ye DJ, et al. CYP1B1 Enhances Cell Proliferation and Metastasis through Induction of EMT and Activation of Wnt/beta-Catenin Signaling via Sp1 Upregulation. PLoS ONE. 2016;11:e0151598.
27. Yoo HM, Kang SH, Kim JY, et al. Modification of ASC1 by UFM1 Is Crucial for ERα Transactivation and Breast Cancer Development. Mol Cell. 2014;56:261–74.
28. Wang K, Chen SY, Wu Y et al. The ufmylation modification of ribosomal protein L10 in the development of pancreatic adenocarcinoma. Cell Death Dis.2023;14.
29. Lin JX, Xie XS, Weng XF et al. UFM1 suppresses invasive activities of gastric cancer cells by attenuating the expression of PDK1 through PI3K/AKT signaling (38, 410, 2019). J Exp Clin Canc Res.2023;42.
30. Ke D, Guo HH, Jiang N, et al. Inhibition of UFM1 expression suppresses cancer progression and is linked to the dismal prognosis and immune infiltration in oral squamous cell carcinoma. Aging-Us. 2023;15:13059–76.
31. Tatsumi K, Sou YS, Tada N, et al. A novel type of E3 ligase for the Ufm1 conjugation system. J Biol Chem. 2010;285:5417–27.
32. Liang JR, Lingeman E, Luong T, et al. A Genome-wide ER-phagy Screen Highlights Key Roles of Mitochondrial Metabolism and ER-Resident UFMylation. Cell. 2020;180:1160–e7720.
33. Mao M, Chen Y, Yang J et al. Modification of PLAC8 by UFM1 affects tumorous proliferation and immune response by impacting PD-L1 levels in triple-negative breast cancer. J Immunother Cancer.2022;10.
34. Wang Z, Gong Y, Peng B, et al. MRE11 UFMylation promotes ATM activation. Nucleic Acids Res. 2019;47:4124–35.
35. Ishimura R, El-Gowily AH, Noshiro D, et al. The UFM1 system regulates ER-phagy through the ufmylation of CYB5R3. Nat Commun. 2022;13:7857.
36. Zhang M, Mathur A, Zhang Y, et al. Mithramycin represses basal and cigarette smoke-induced expression of ABCG2 and inhibits stem cell signaling in lung and esophageal cancer cells. Cancer Res. 2012;72:4178–92.
37. Zhao Y, Zhang W, Guo Z, et al. Inhibition of the transcription factor Sp1 suppresses colon cancer stem cell growth and induces apoptosis in vitro and in nude mouse xenografts. Oncol Rep. 2013;30:1782–92.
38. Quarni W, Dutta R, Green R et al. Mithramycin A Inhibits Colorectal Cancer Growth by Targeting Cancer Stem Cells. Sci Rep-Uk. 2019;9.
39. Saha S, Mukherjee S, Mazumdar M, et al. Mithramycin A sensitizes therapy-resistant breast cancer stem cells toward genotoxic drug doxorubicin. Transl Res. 2015;165:558–77.
40. Tornin J, Martinez-Cruzado L, Santos L, et al. Inhibition of SP1 by the mithramycin analog EC-8042 efficiently targets tumor initiating cells in sarcoma. Oncotarget. 2016;7:30935–50.
41. Chang KY, Huang CT, Hsu TI, et al. Stress stimuli induce cancer-stemness gene expression via Sp1 activation leading to therapeutic resistance in glioblastoma. Biochem Biophys Res Commun. 2017;493:14–9.
42. Shen HT, Chien PJ, Chen SH et al. BMI1-Mediated Pemetrexed Resistance in Non-Small Cell Lung Cancer Cells Is Associated with Increased SP1 Activation and Cancer Stemness. Cancers. 2020;12.
43. Kennedy BJ. Metabolic and Toxic Effects of Mithramycin during Tumor Therapy. Am J Med. 1970;49:494–.
44. Pérez M, Baig I, Braña AF et al. Generation of New Derivatives of the Antitumor Antibiotic Mithramycin by Altering the Glycosylation Pattern through Combinatorial Biosynthesis. Chembiochem. 2008;9:2295 – 304.
45. Remsing LL, González AM, Nur-e-Alam M, et al. Mithramycin SK, a novel antitumor drug with improved therapeutic index, mithramycin SA, and demycarosyl-mithramycin SK:: Three new products generated in the mithramycin producer through combinatorial biosynthesis. J Am Chem Soc. 2003;125:5745–53.
46. Shinde D, Albin D, Zoma M, et al. Transcriptional Reprogramming and Inhibition of Tumor-propagating Stem-like Cells by EC-8042 in ERG-positive Prostate Cancer. Eur Urol Oncol. 2019;2:415–24.
47. Hermida-Prado F, Villaronga MA, Granda-Díaz R et al. The SRC Inhibitor Dasatinib Induces Stem Cell-Like Properties in Head and Neck Cancer Cells that are Effectively Counteracted by the Mithralog EC-8042. J Clin Med. 2019;8.
48. Dutta R, Khalil R, Mayilsamy K et al. Combination Therapy of Mithramycin A and Immune Checkpoint Inhibitor for the Treatment of Colorectal Cancer in an Orthotopic Murine Model. Front Immunol. 2021;12.
49. Estupiñán O, Rendueles C, Suárez P et al. Nano-Encapsulation of Mithramycin in Transfersomes and Polymeric Micelles for the Treatment of Sarcomas. J Clin Med. 2021;10.
50. Wang J, Kang M, Wen Q, et al. Berberine sensitizes nasopharyngeal carcinoma cells to radiation through inhibition of Sp1 and EMT. Oncol Rep. 2017;37:2425–32.
51. Kumari S, Banerjee S, Kumar M et al. Overexpression of UBA5 in Cells Mimics the Phenotype of Cells Lacking UBA5. Int J Mol Sci. 2022;23.
52. Zhou JZ, Ma XH, He XR et al. Dysregulation of PD-L1 by UFMylation imparts tumor immune evasion and identified as a potential therapeutic target (120, e2215732120, 2023). P Natl Acad Sci USA. 2023;120.
53. Balce DR, Wang YT, McAllaster MR et al. UFMylation inhibits the proinflammatory capacity of interferon-γ-activated macrophages. P Natl Acad Sci USA. 2021;118.
54. Song M, Yeku OO, Rafiq S et al. Tumor derived UBR5 promotes ovarian cancer growth and metastasis through inducing immunosuppressive macrophages. Nat Commun. 2020;11.
55. Wang X, Zhou T, Yang X, et al. DDRGK1 Enhances Osteosarcoma Chemoresistance via Inhibiting KEAP1-Mediated NRF2 Ubiquitination. Adv Sci (Weinh). 2023;10:e2204438.

Publisher's note